Conceptual model of recharge to southeastern Badain Jaran Desert groundwater and lakes from environmental tracers

John B Gates[a1], W Mike Edmunds[a], W George Darling[b], Jinzhu Ma[c], Zhonghe Pang[d], and Adam A Young[e]

a *Oxford Centre for Water Research, University of, Oxford, OX1 3QY, UK*

[b] *British Geological Survey, Maclean Building, Crowmarsh Gifford, Wallingford, OX10 8BB, UK*

[c] *Key Laboratory of Western China's Environmental System (Ministry of Education), Lanzhou University, 222 South Tainshui Road, Lanzhou 730000, China*

[d] *Institute of Geology & Geophysics, Chinese Academy of Sciences, P.O. Box 9825, Beijing 100029, China*

[e] *Environmental Change Research Centre, University College London, Gower Street, London WC1E 6BT, UK*

Abstract

Sources of groundwater recharge to the Badain Jaran Desert in China have been investigated using geochemical and isotopic techniques. Stable isotope compositions (δ^{18}O and δ^2H) of shallow groundwater and surface water from oasis lakes evolve from a starting composition considerably depleted compared to local unsaturated zone moisture, confirming inferences from Cl mass balance that direct infiltration of precipitation is not a volumetrically-important source of recharge to the shallow aquifer in the study area. Shallow phreatic and deeper confined groundwater bodies appear unconnected based on chemical composition and radiocarbon activities. Hydrogeologic evidence points toward a bordering mountain range (Yabulai) as a likely recharge zone, which is consistent with tracer results. A mean residence time in the range

---

[1] *Corresponding Author: john.gates@stcatz.oxon.org*

1-2 ka for the desert's southeastern margin is inferred from radiocarbon. These results reveal that some replenishment to the desert aquifer is occurring but at a rate much lower than previously suggested, which is relevant for water resources planning in this ecologically-sensitive area.

Key Words: China, arid regions, groundwater recharge, environmental isotopes, water resources

1 Introduction

Approximately 22% of China's land surface is desert (Zhao, 1986). This represents an area of 2.1 million km^2, roughly the same size as the Arabian deserts, or as Western Europe. Along with low soil fertility and extreme climate, fresh water scarcity is a limiting factor for agriculture and economic development in this region, which presently contains only 2% of the Chinese population despite its large extent. There is current bureaucratic focus on settlement and development of China's mainly arid western provinces, which are less economically developed relative to eastern China. However, the environmental challenges of this development have become apparent from high rates of desertification, falling water tables and soil salinization, and some villages and agricultural lands have been abandoned due to a combination of these factors.

Shallow groundwater is the primary water resource for sparse settlements and subsistence agriculture in the Badain Jaran Desert in northwestern China, which is well-known domestically for its pristine landscape of tall sand dunes and desert lakes. At present, much about the sources and characteristics of the desert's shallow groundwater remains poorly understood as a result of the area's isolation and relatively low water demand. However, groundwater abstraction is increasing in nearby areas and the need for easily accessible fresh water could extend pumping to the desert or hydraulically connected areas, potentially threatening livelihoods and a unique oasis ecosystem which is dependent upon groundwater. The aim of this study is to establish a conceptual model of sources and timing of recharge to the shallow Quaternary aquifer of the

Badain Jaran Desert using environmental tracers including ion chemistry, stable isotopes of water, radiocarbon and tritium.

2 Study Area

The Badain Jaran Desert (39°20'N to 41°30'N and 100°E to 104°E) spans approximately 50,000 km² within the Alashan Plateau and is considered to be the fourth largest desert in China (**Fig 1**). It is bordered by mountain ranges to the south and southeast (the Heishantou and Yabulai Mountains, respectively), and the lowland areas of the Gurinai grassland and the Guezi Hu lacustrine plains to the west and north. Settlement is currently sparse and land use limited to subsistence agriculture and grazing. The landscape consists primarily of unconsolidated sand dunes, the largest of which tend to be oriented in SW-NE trending rows and, despite only very sparse vegetation, can exceed 400 m in height. The dune sands are derived primarily from lacustrine and fluvial sediments of the Heihe River basin which were exposed by declining surface water levels subsequent to the last glacial maximum approximately 30 ka years BP (Yan *et al.*, 2001). The sediments were transported during intermittent periods of high aeolian activity and predominantly westerly winds during the Holocene. This climatic variability has also been cited as a possible factor in the growth of abnormally large "megadunes" as a result of alternation of periods of dune accumulation during arid phases with periods of dune stabilization during humid phases due to surface calcification (Dong *et al.*, 2004, Yang, 2000).

Figure 1 Map of groundwater sample locations

The dunes are interspersed with lakes that occur in many low-lying areas throughout the desert and vary in size, shape and salinity. The densest occurrence of lakes is in the southeastern section of the desert, with more than 100 concentrated within an area of about 4,000 km². The lakes are groundwater-fed and have no surface water outflows or inflows. Radiocarbon dating of palaeo-

shorelines has shown that lake levels have varied significantly over the last 10,000 years and were as high as 15 m above their current position 4-6 ka BP (Yang and Williams, 2003), which may represent the end of the Holocene humidity optimum in this area though the timing of this event is unclear (An *et al.*, 2000).

The geological succession below recent aeolian dune formations remains poorly characterized. The Badain Jaran lies in one of several basin depressions of the Alashan tectonic block which formed during the Late Jurassic and Early Cretaceous from strike-slip and localized extensional deformations associated with the Lhasa block-Asia collision (Vincent and Allen, 1999). Abundant faulting related to Altyn Tagh and Qilian Shan fault structures is evident surrounding the desert and is presumably present below the dune field as well. Sedimentary rocks of Jurassic, Cretaceous and Tertiary age outcrop near the southern margin of the desert, and granites of the Yabulai Mountain range are prominent in the desert-mountain transition in the southeast. Extensive alluvial features of Quaternary origin are apparent in the Heishantou and Yabulai Mountain piedmont areas. An outcropping anticline structure within the southeastern section of the dune field also contains fanglomerates, silts and interbedded carbonates (Hofmann, 1999).

The desert's only borehole (sample ID WBD5, 80 m depth), constructed near Baddam Lake in 2005, illustrates that the Quaternary dune sands comprise a shallow phreatic aquifer. The unconsolidated sands are interlayered with fine-grained lacustrine deposits derived from palaeolakes, which result in locally confined aquifer conditions apparent from artesian springs and strong vertical salinity gradients in some lakes. Granitiods of the Yabulai Mountain block are present at the base of this borehole, and may provide a lower confining unit for the shallow aquifer in this area, whereas Cretaceous sandstone likely underlies most Quaternary deposits away from the mountain margin and may serve as a second water-bearing stratum. In the absence of additional boreholes, lake levels serve as a natural piezometer network for water table depths

and approximation of groundwater flow directions. Recorded water table elevations at the base of unsaturated zone cores confirm that lake levels are accurate indicators of regional water table levels in most locations (Gates *et al.*, in press). Current lake elevations trend from highest in the southeast (>1300 m asl) to less than 1100 m asl in the west, mirroring the general trend in topography and suggesting the Gurinai area and the lower Heihe River basin as possible discharge zones (**Fig 2**). The Heihe River, which runs from south to north and is the only major surface water source near the desert, is down-gradient of desert water tables and is therefore not considered a possible source of recharge.

Figure 2 Lake level contours (50 m) in the southeastern Badain Jaran

Climatically the area is strongly continental and is regarded as a cold desert. Daily daytime temperatures in summer months range up to 40°C, and mean monthly temperatures fall to -10°C in January and sub-zero minimum temperatures prevail for most of the year. The southeastern Badain Jaran is near the current northern extent of the East Asian monsoon which provides the primary source of precipitation, 70% of which falls from July to September. Cold and dry continental air masses from prevailing westerly winds dominate in winter. Mean annual precipitation measured at the nearest meteorological station (Zhongqanzi Station, 20 km southeast of the study area) was 84 mm from 1956-1999 and is highly variable (coefficient of variation 0.39), and potential evaporation from surface water is ~2600 mm/yr (Ma *et al.*, 2003). Average precipitation decreases significantly from south to north across the desert, declining to about 50 mm/yr at Wentugaole near the border between China and Mongolia (Domros and Peng, 1988) due to progressively declining influence of monsoonal moisture. Orographic effects result in slightly higher rainfall rates in the Yabulai Mountains (150 mm/yr).

3 Previous Studies

Several studies have addressed the question of recharge to shallow groundwater in this area. On the basis of lake and groundwater salinities Hofmann (1999) suggests the presence of two hydraulically disconnected flow systems, one to the north of an anticline approximately 40 km from the desert's southern boundary fed by direct recharge, and one to the south fed by a source external to the dune field. A diffuse recharge rate of 20 mm/yr was estimated from the input volume needed to offset lake evaporation. Yang and Williams (2003) and Jäkel (2002) also hypothesize that direct recharge may be an important groundwater source. However, subsequent Cl mass balance estimates of direct recharge of the order of 1 mm/yr challenge this scenario (Gates *et al.*, in press). Chen *et al.* (2004) propose rapid transfer of snow melt from the Qilian Mountains (200 km southwest) through fracture networks to the desert, although hydrogeologic considerations render this highly unlikely (interbasin flow against the prevailing NW-SE strike of faulting), and packer test samples of deep groundwater in these fault zones show palaeowater characteristics (Pang *et al.*, 2007). Ma and Edmunds (2006) argue for a palaeowater origin for shallow groundwater in the area of Baddam Lake using evidence from chemical and stable isotope studies from this area and analogous data from the nearby Minqin Basin (Edmunds *et al*, 2006).

At the desert's southeastern margin, Yang (2006) reports major ion and tritium data from groundwater in the vicinity of the Yabulai Mountains which suggest recent recharge of local infiltration. The Gurinai area to the west of the desert has also been the focus of hydrological investigations (for example, Geyh and Gu, 1992, Wen *et al.*, 2005, Zhang *et al.*, 2005) and has been included in numerous studies of the lower Heihe River (Chen *et al.*, 2006, Feng *et al.*, 2004). Sources of shallow groundwater appear to be widely variable, possibly include seepage from the Heihe River and local irrigation returns, and deep groundwaters mostly have ages in the thousands of years based on radiocarbon (Chen *et al.*, 2006).

4 Methods

Water samples were obtained in 2004 and 2005 in the southeastern Badain Jaran Desert and in nearby vicinities to the south including the northwestern side of the Yabulai mountain range (labeled *mountain front* in **Table 1**), the southern margin of the desert including the Heishantou mountain range (labeled *southern margin* in **Table 1**) as well as from the areas of Gurinai and Xugue (**Fig 1**). Because the study area contains only sparse settlement and therefore a limited number of sampling points, the sampling strategy was opportunistic and included wells, springs, lakes and rainfall events. Samples of shallow phreatic groundwater (labeled *shallow* in **Table 1**) are typically from wells <5 m deep but up to 83 m in the case of sample WBD5. The wells tend to be lined with stones or brick and have saturated thicknesses of 1-2 m. Most are located in low-lying areas with water tables less than 2 m below surface. Wells were purged with a submersible pump for at least 20 minutes before sample collection. Samples of underlying (usually confined) units (labeled *deep* in **Table 1**) are primarily from irrigation wells and are open over intervals of several meters. None are present in the dune field therefore the locations reported here are the nearest available. All had been discharging continuously for hours or days prior to sampling. In addition one unsaturated zone profile was collected to characterize isotopic compositions of vadose zone pore water.

Samples for major ion chemistry were collected in Nalgene bottles pre-washed with 5% HNO_3 solution. Samples were filtered at 0.45 μm and samples for cation analysis were stabilized with addition of 1% HNO_3. Unfiltered samples for radiocarbon and stable isotope analysis were also collected at this time using a submersible pump and stored in airtight HDPE bottles. Unsaturated zone samples were collected to a depth of 10 m by hand auger, and moisture was extracted from sediment pore space by azeotropic distillation with toluene (Revesz and Woods, 1990). Field measurements included pH, dissolved oxygen, temperature, and bicarbonate alkalinity by titration.

Major anions (Cl^-, SO_4^{2-}, HCO_3^- and NO_3^-) were analyzed at the Oxford University Centre for the Environment by ion chromatography (Dionex DX-500). Analytical precision was 3% of concentration based on reproducibility of samples and the detection limit was 0.1 mg/L for undiluted samples. Cations and selected trace elements were analyzed at NERC ICP-AES facility at Royal Holloway, University of London (Optima 3300RL ICP-AES). All groundwater chemistry results were within 5% ionic charge balance. Stable isotopes of water ($\delta^{18}O$ and δ^2H) in groundwater and rainfall were analyzed at the British Geological Survey Isotope Laboratory in Wallingford UK by isotope ratio mass spectrometry. Precisions were ±0.2‰ for $\delta^{18}O$ and ±2‰ for δ^2H. Radiocarbon samples were prepared and analyzed at the NERC Radiocarbon Laboratory in East Kilbride UK. Dissolved inorganic carbon (DIC) was reacted with 85% orthophosphoric acid to CO_2, graphitized, and ^{14}C was measured with AMS. Percent modern carbon values (pmC) had 1σ errors <0.5 in all cases. $\delta^{13}C$ was measured with a stable isotope mass spectrometer (VG Optima) with an overall analytical error of ±0.5‰ based on repeated analysis of samples and standard materials. Tritium measurements were performed at the Groundwater Tracing Laboratory of the Institute of Geology and Geophysics, Chinese Academy of Sciences in Beijing. Water samples were first distilled to remove salts, and then tritium was enriched electrolystically by a factor of 20. Counting was performed on a Quantlus 1220 liquid scintillation counter. The achieved precision was +/- 0.3 TU.

5 Results

Shallow groundwater samples are characterized by a high degree of variability with respect to total dissolved solids (TDS), which ranges from 0.39 g/L (SBD-11) to 6.1 g/L (W40). On average, Badain Jaran dune field groundwaters have lower TDS than any other area. In general samples have neutral to slightly alkaline pH (7.3 to 8.5), with the exception of one shallow sample with pH 6.0 (W32). The desert groundwaters are also variable in major ion composition,

though generally Na + K rich with no dominant anion type (**Fig 3a**). One outlier is a flowing spring that empties into Lake Huhejaran (SBD11) which has low $Cl/(SO_4+HCO_3)$ in comparison. Deep wells to the south of the Yabulai Mountains have ionic compositions similar to Yabulai/desert margin wells, as do samples from the Zhoujiajiang area. Two pairs of samples are distinct from this group. Wells W28 and W29 from the Jinchang area are more abundant in Ca and HCO_3, and samples W27 (Zhoujiajiang) and W1 (Yabulai Town) are more abundant in Ca without high HCO_3 (**Fig 3b**). The well samples >200 m depth plot slightly to the right of Badain Jaran wells due to greater influence of Na+K and Cl. Neither total mineralization nor major ion composition are clearly distinguishable between geographic groups. Dissolved oxygen concentrations >2 mg/L in most cases illustrate prevailing aerobic conditions for shallow and deep confined groundwater (measurements for Badain Jaran dune field samples not available). This is confirmed by the presence of high NO_3 as well as low concentrations of the redox-sensitive elements Fe and Mn (**Table 1**). One exception is sample W4 which has low dissolved oxygen, high Fe and Mn and low NO_3 indicative of reducing conditions (detectable levels of Mn and Fe in rainfall show that atmospheric deposition also contributes to observed concentrations in groundwater). Occurrence of some denitrification in the area has been previously identified (Gates *et al.*, 2008).

Figure 3a Piper diagram comparing Badain Jaran, Yabulai mountain front and rainfall samples

Figure 3b Piper diagram comparing deep and shallow groundwater samples

Stable isotope values of groundwater range from -91.5 to -13.4 $\delta^{18}O$ and tend to cluster by both geographic location and well depth (**Fig 4**). Lakes and unsaturated zone samples both tend to be heavier than groundwater in $\delta^{18}O$ and δ^2H due to evaporative enrichment. Rainfall events sampled in the Badain Jaran in 1999, 2005 and 2006 range from -4.8 to -0.6‰ $\delta^{18}O$, within the observed range for groundwater. Radiocarbon activities range from 2.7 to 101.8 pmC and $\delta^{13}C$

from -4.5 to -10.1‰ (**Table 2**). Radiocarbon activities fall into two groups according to well depth, with shallow wells between 60 and 102 pmC and deep wells (>100 m) between 2.7 and 48 pmC. The lowest activity is found in the water supply well of Zhoujiajiang (W23). Shallow wells from the Xugue area and the Yabulai mountain/desert margin conform to the same general patterns. Tritium activities for 10 samples range from non-detect (W37, W43 and WBD5) up to 43.2 TU (W34).

Figure 4 $\delta^{18}O$ - δ^2H diagram

6 Discussion

6.1 Recharge Source Areas

Direct (diffuse) recharge within the dune field has been shown to be minimal (Gates *et al.*, in press), suggesting that base flow from outside the dune field supplies the desert's shallow groundwater. Head gradients commencing at the Yabulai Mountains and diminishing to the west and northwest suggest a flowpath from this mountain range towards the desert interior (**Fig 2**). High radiocarbon (78-97 pmC) and tritium (12.1-43.2 TU) activities of groundwater at the mountain front (samples W8, W9, W10, W33 and W34) are consistent with active recharge in the area. Physical evidence of active recharge is present in the form of a small perennial stream hosted in a palaeo-river channel terminating near Zhongqanzi. The fact that flow persists through most dry seasons implies a component of groundwater-fed base flow.

Close correspondence in major ion compositions in Yabulai mountain front and southeastern Badain Jaran groundwaters is also consistent with a common hydrogeochemical history of the two areas (**Fig 3a**). In both cases, evaporation is the primary control on Cl in the absence of geologic sources in the study area. Significant evaporite salt deposits are actually present in the vicinity of Yabulai Town where they are commercially extracted, but while leaching into shallow

groundwater is possible locally there is no indication of broader impacts on groundwater salinity. Strong linear relationships with Cl illustrate that Na and SO_4 variability is also largely determined by evaporation rather than mineral dissolution or ion exchange (**Figs 5a and 5b**).

Figure 5a Groundwater Na/Cl cross-plot

Figure 5b Groundwater SO_4/Cl cross-plot

Stable isotope relationships also support the possibility of connections between desert shallow groundwaters and some of those of the surrounding region. A local meteoric water line (LMWL) for Zhangye (the nearest Global Network of Isotopes in Precipitation (GNIP) monitoring station, approximately 250 km to the southwest of the study area; IAEA/WMO, 2007; **Fig 4**) provides the basis for this analysis. Regression on the Zhangye precipitation records yields a $\delta^2H/\delta^{18}O$ slope of 7.32 and deuterium intercept of +1.1 (r^2=0.96 for 68 records representing intermittent periods between 1986 and 2001). Annual weighted means of sampled events plot near the LMWL and all but one year group at approximately -7‰ $\delta^{18}O$.

While there is a high degree of variability between individual storms, winter precipitation is generally more depleted than summer, with mean December precipitation depleted by 17‰ $\delta^{18}O$ compared to the mean for August (**Fig 6**). This likely stems from the greater role of westerly air masses in winter months which contribute less moisture overall and are strongly depleted by continentality and low temperature. Annual weighted means closely reflect summer isotopic signatures because the majority of annual precipitation is derived from the East Asian monsoon during summer months. One heavy rainfall event sampled in the Badain Jaran Desert in September 1999, which probably represented a significant proportion of the annual total, was similar to the September mean rainfall composition of Zhangye (Ma and Edmunds, 2006).

Figure 6 Monthly weighted mean isotope compositions for Zhangye GNIP station (icon size
scaled to monthly amounts)

Shallow groundwater from the Badain Jaran dune field is enriched (to between -5.4 and -2.0‰
$\delta^{18}O$) along an evaporation line of slope +4.7 which is shared with lake samples. Lake samples
are more enriched than groundwater as a result of evaporation from the lake surface, a process
also reflected in salinities higher than groundwater. The lake/groundwater evaporation line
intercepts the LMWL at approximately -12‰ $\delta^{18}O$, which is 5‰ more depleted than Zhangye
weighted means. Isotopic patterns relative to Badain Jaran groundwater can be summarized as
follows:

a) Badain Jaran unsaturated zone moisture samples are enriched to values between +2.7 and
+15.5‰ $\delta^{18}O$ along a line of slope 2.4 that intercepts the LMWL at -7‰ $\delta^{18}O$. The low slope is
indicative of kinetic fractionation effects of evaporation from pore moisture of unsaturated
sediments (Barnes and Allison, 1988, Clark and Fritz, 1997). The isotopic correspondence
between weighted mean rainfall and the LMWL origin for the unsaturated zone evaporation line
entails that the pore waters have evolved from meteoric water of a similar isotopic composition to
modern desert rainfall. It also suggests that direct infiltration is not a major source of recharge to
the southeastern Badain Jaran dune field because the meteoric water intercept is distinctly lighter.
The disconnect has also been argued based on chloride mass balance studies (Gates *et al.*, in
press).

b) Isotopic compositions of shallow groundwater samples from the areas of Xugue (east of the
desert) and Gurinai (west of the desert) tend to conform to the same pattern as the dune field
samples. They have evolved from meteoric water similar to the Badain Jaran samples and have
been similarly enriched by evaporation. Gurinai is most likely a discharge zone for the Badain

Jaran shallow aquifer considering regional hydraulic head patterns and Xugue may be fed by the same recharge source(s) and be hydraulically connected to the dune field.

c) Yabulai mountain front samples with high radiocarbon activities representative of modern or recent recharge have LMWL intercept more depleted than the Zhangye precipitation mean (-10‰ $\delta^{18}O$). This discrepancy in meteoric water source could result from altitude differences producing isotopically lighter rainfall with increasing elevation. The peak elevation of the Yabulai Mountains is ~300 m above the elevation of Zhangye; this $\delta^{18}O$-altitude gradient would be within the range of those observed elsewhere (Clark and Fritz, 1997).

The Yabulai mountain front samples plot along an evaporation line of similar $\delta^{2}H/\delta^{18}O$ slope and degree of evaporative enrichment, but with LMWL intercept of -10‰ $\delta^{18}O$, which is approximately 2‰ heavier than the Badain Jaran samples. This pattern is considered consistent with the Yabulai Mountains as a source of recharge to the desert allowing for possible shifts in meteoric input signals associated with climatic variability (see Section 6.2 on recharge time scale). For example a 2‰ depletion in $\delta^{18}O$ between 1,000 years BP and the present is roughly consistent with the $\delta^{18}O$ trend portrayed in the Guliya ice core (northern Tibetan Plateau) over the same time period, possibly attributable to atmospheric warming (Thompson *et al.*, 2006).

d) Deep groundwaters tend to be more depleted on average (mean -10‰ $\delta^{18}O$) than shallow groundwaters, and primarily conform to meteoric slope, the exceptions being W43 (Gurinai) and W37 (Xugue). The range for deep wells extends to -12‰ $\delta^{18}O$, near the intercept of meteoric and Badain Jaran evaporation lines. However upwelling from deeper formations as a major source of desert shallow groundwater is inconsistent with Cl concentrations in Badain Jaran shallow groundwaters, which are consistently lower than most deep groundwater samples.

A positive relationship between $\delta^{18}O$ and radiocarbon activity is apparent for some deep groundwater samples from southern sections of the study area which lie along the LMWL, similar to a pattern observed in the Minqin Basin (**Fig 7**). Ma and Edmunds (2006) argue that this relationship results from climatic trends since the late Pleistocene. In particular, Pleistocene age groundwaters in Minqin (Edmunds *et al.*, 2006) and the North China Plain (Zongyu *et al.*, 2003) show $\delta^{18}O$ values of -9.5 to -10.6‰, and -9.4 to -11.7‰, respectively, which is ~4‰ lighter than modern rainfall. Noble gas recharge temperatures of waters of this age are mainly 4 but as much as 6-9 degrees C cooler than modern recharge for both of these areas, similar to the ratio of 0.58‰ $\delta^{18}O$ enrichment per degree C of warming in globally-averaged $\delta^{18}O$-temperature relationships (Rozanski *et al.*, 1993). Comparable temperature differences have also been suggested by pollen and glacial records (Yang *et al.*, 2004, Zhou *et al.*, 2001). This pattern does not hold for any samples (deep or shallow) within or adjacent to the dune field (WBD5, W37, W43 and Yabulai mountain front locations), which may reflect a difference in geographic source of recharge.

Figure 7 $\delta^{18}O$ versus pmC (including data from Edmunds et al 2006). Values for samples which have been subject to evaporation have been adjusted to reflect original meteoric water.

e) Shallow groundwaters of the desert's southern margin in areas surrounding the town of Youqi and the Heishantou Mountains are wide-ranging particularly in δ^2H, which varies from -39 to -76‰. These tend to have meteoric origins more representative of Zhangye rainfall than the Badain Jaran wells.

6.2 Recharge Chronology

High tritium activities distinguish Yabulai mountain front groundwater from Badain Jaran samples WBD5 and deep well samples W37 and W43 in which tritium was not detected. While quantitative tritium dating is subject to many uncertainties in this case, residence times of generally less than ~50 years may be inferred for samples exceeding 20 TU (Ma *et al.*, in press). For pre-modern groundwaters, age corrections of radiocarbon can provide residence time estimates.

High radiocarbon activities in the high tritium samples of the Yabulai mountain front illustrate that little or no dilution of radiocarbon activities occurs during recharge (up to 102 pmC). The high activities most likely signify gaseous CO_2 in the unsaturated zone as the predominant source of DIC to recharging groundwater considering the scarcity of carbonates in silicate sands and granite outcrops through which recharge may occur, although carbonate dissolution from fluvial and lacustrine facies, and presumably minor amounts present in sands and sandstones, and subsequent re-equilibration with soil CO_2 under open-system conditions is also possible.

The equilibrium $\delta^{13}C$ CO_2(g)–DIC fractionation factor (a function of temperature; (Mook *et al.*, 1974) entails an enrichment of approximately 9‰ in DIC relative to gaseous CO_2 for 20 °C. Assuming that the sample with highest pmC value (W40) is representative of recharging waters and that calcite dissolution is negligible, then gaseous CO_2 in the unsaturated zone would have a value of ~18‰ $\delta^{13}C$. This value is between expected values for soil gas in soils hosting C_3 (-23‰) and C_4 vegetation (-12.5‰) (Aravena *et al.*, 1992, Vogel, 1993), and a similar value has been found elsewhere in arid China (Zongyu *et al.*, 2003). While C_3 plants comprise the vast majority worldwide (approximately 90%), C_4 plants are prominent in cold arid environments (Pyankov *et al.*, 2000), and several C_4-pathway shrubs including *Haloxylon ammodendron* have been documented as important species in the Alashan Plateau (Kürschner, 2004, Wang, 2007).

Calcite saturation indices were calculated using PHREEQC (Parkhurst, 1995) and indicate that groundwater samples from the hypothesized recharge area are saturated with respect to calcite in all cases (**Table 2**). Hence saturation is likely reached during recharge (under open system conditions with respect to atmospheric CO_2 and therefore without much alteration of pH). Low infiltration rates shown by elevated Cl^- concentrations may allow for calcite saturation without the presence of significant solid phase carbonates by allowing enough time for CO_2-DIC equilibration during infiltration and providing a source of Ca^{2+} from evaporative enrichment in the near surface with possible additional contributions from silicate weathering.

Below the water table closed-system conditions prevail due to isolation from the atmosphere. Solid carbonates in the aquifer matrix including interbedded lacustrine deposits (Gao *et al.*, 2006) likely contribute to DIC. Several samples also have molar $Mg^{2+}/Ca^{2+}>1$, possibly indicative of influence by mafic minerals considering the absence of dolomite. Congruent dissolution, however, is not expected to occur in this case because of calcite saturation during recharge, although incongruent reactions may allow cation and carbon isotopic exchange under dynamic equilibrium conditions. This is consistent with the lack of correlation between bicarbonate alkalinity and pmC. Nonetheless, $\delta^{13}C$ values for DIC are inversely correlated with pmC for shallow mountain front and dune field samples, suggesting that isotopic evolution is occurring in their case (**Fig 8**). This relationship may be explained by equilibrium isotopic exchange between DIC and the solid phase bicarbonate ($\sim$ +2‰ $\delta^{13}C$; Hofmann, 1999) due to incongruent dissolution, which can occur at calcite saturation and progressively enriches $\delta^{13}C_{DIC}$ and dilutes active radiocarbon (Turner, 1982, Wigley *et al.*, 1978). $\delta^{13}C_{DIC}$ evolves to a value of approximately -7‰, consistent with freshwater carbonates.

Figure 8 Groundwater $\delta^{13}C_{DIC}$/pmC cross-plot

A modified version of the Pearson (1965) isotopic correction model (as presented by Clark and Fritz, 1997) is used to account for isotopic dilution from incongruent dissolution of carbonates. The radiocarbon dilution factor q is calculated based on the change in DIC δ^{13}C between the sample and the recharge zone by the equation:

$$q = \frac{\delta^{13}C_{DIC} - \delta^{13}C_{carb}}{\delta^{13}C_{rech} - \delta^{13}C_{carb}} \quad \text{(Eq 1)}$$

where the subscripts *carb* and *rech* represent solid-phase carbonate and recharging water, respectively. $\delta^{13}C_{rech}$ can be calculated as:

$$\delta^{13}C_{rech} = \delta^{13}C_{soil} + \varepsilon^{13}C_{DIC-CO2(soil)} \quad \text{(Eq 2)}$$

where ε^{13}C is the fractionation factor between DIC and soil CO$_2$. However because $\delta^{13}C_{soil}$ was estimated using the approach of Mook *et al.* (1974) using sample W34 as representative of $\delta^{13}C_{rech}$, $\delta^{13}C_{rech}$ is specified directly.

The mean of calculated q-values (0.76) is intermediate between the ranges reported by Vogel (1970) for carbonate aquifers ($0.65 < q < 0.75$) and sedimentary basins with trace carbonates ($0.75 < q < 0.9$) (**Table 2**). The model yields reasonable q-values and ages for the recharge zone (positive in the hundreds of years). Extreme q-values (greater than one or less than 0.65) are portrayed for a small number of deep well samples (W20, W27 and W43). In these cases, the model inputs, which are specific to the Yabulai Mountains at the present day, may not be representative of recharge sources because of differing climate, vegetation and/or geologic factors.

Resulting groundwater ages are relatively young (0-650 years) for shallow wells near the Yabulai Mountains. The southeastern Badain Jaran Desert sample (WBD5) has a model age of approximately 1600 years. This is consistent with calculations of transit time from the Yabulai mountain front to the southeastern Badain Jaran Desert based on Darcy's Law, which suggests approximately 1,000 years to Baddam Lake given observed hydraulic head values and assuming a hydraulic conductivity of $1.33 *10^{-4}$ m/s for unconsolidated sand based on the grain size distributions of dune sands (Masch and Denny, 1966).

Among deep wells, at least three samples (W23, W25 and W26) indicate ages > 20 ka, all located slightly to the north of the village Zhoujiajiang. Holocene or late Pleistocene ages for deep groundwaters are found in all other areas: the Youqi area (11,000, 11,500 and 14,000 years), Yabulai Town (7,500 and 8,500 years), Gurinai (13,000), Xugue (4,000) and Jinchang (8,000 and 5,000). One well near Jinchang (W29) has 72.5 pmC, which may signify a component of irrigation return in this intensively cultivated area. NO_3^-/Cl^- is significantly higher in W-29 than any other deep well, indicating possible nutrient addition from fertilizers. Shallow groundwater in Gurinai sample W44 had a high pmC value, which indicates relatively recent recharge from surface water or irrigation. Sample W40 within the desert margin also had anomalously high pmC and high TDS which may be indicative of return from well extraction or other localized infiltration.

6.3 Lake/Groundwater Interaction

Stable isotope signatures from the desert's lakes illustrate the close connection with the shallow groundwater (**Table 3**). The common evaporation line confirms that the lakes are fed by shallow groundwater, and additional evaporation from surface water is demonstrated by further enrichment along the evaporation line. The timing of evaporative displacement from the LMWL

of Badain Jaran shallow groundwaters is unclear and could have included evaporation directly from the water table in shallow locations, during recharge, or at the well head prior to sampling. The latter explanation cannot be ruled out because desert wells typically have wide diameters and are sparsely used.

Differing degrees of enrichment of both stable isotopes and TDS amongst lakes suggests variable losses due to evaporation. Because the lakes have no surface inflow or outflow, potential water losses are limited to evapotranspiration and seepage return to groundwater. Hence, the amount of seepage to groundwater may be determined by stable isotope balance estimation of evaporation losses. The hypothetical limiting isotopic composition of lake water undergoing full evaporation (desiccation) is given by

$$\delta^* = \frac{(h \cdot \delta_A) + \varepsilon}{h - (\varepsilon \cdot 10^{-3})}, \quad \text{(Eq 3)}$$

where h is atmospheric relative humidity, δ_A is the isotopic composition of atmospheric water vapor ambient to the lake and ε is the isotopic fractionation factor consisting of an equilibrium (ε^*) and a kinetic (ε_K) component (Gat and Levy, 1978). The fractionation factors ε^* and ε_K are dependent upon local temperature and humidity conditions, respectively and are calculated using empirical relationships (Gonfiantini, 1986, Horita and Wesolowski, 1994). Relative humidity is specified as the mean for summer months in Youqi as most representative of peak evaporation conditions (i.e. flux-weighted). In the absence of direct measurement, δ_A is often estimated assuming isotopic equilibrium with local precipitation. While generally effective in humid regions, this assumption may not be appropriate in some arid conditions due to the influence of locally-recycled moisture (Gibson *et al.*, 1999, Krabbenhoft *et al.*, 1990). Because both the local

evaporation line and LMWL are well-defined for the study area, δ_A may be calculated from the expression for the slope of the LEL (Gat, 1996):

$$S_{LEL} = \frac{h(\delta_{AH} - \delta_{IH}) + \varepsilon_H}{h(\delta_{AO} - \delta_{IO}) + \varepsilon_O}, \quad \text{(Eq 4)}$$

where δ_I is the isotopic composition of incoming groundwater, and subscripts H and O denote values for δ^2H and $\delta^{18}O$, respectively. Assuming that ambient water vapor will generally conform to the LMWL, the substitution

$$\delta_{AH} = S_{LMWL} \cdot \delta_{AO} + D_{LMWL} \quad \text{(Eq 5)}$$

is made for slope S_{LMWL} and deuterium intercept D_{LMWL} of the LMWL. Solving Eq 4 for $\delta_{AO,}$

$$\delta_{AO} = \frac{S_{LEL}(h \cdot \delta_{IO} - \varepsilon_O) + \varepsilon_H + D_{LMWL} \cdot h - \delta_{IH} \cdot h}{h(S_{LEL} - S_{LMWL})}. \quad \text{(Eq 6)}$$

Isotopic composition of incoming groundwater is set equal to that of flux-weighted rainfall inputs according to the intercept of the LMWL and LEL. This assumes that there is no chain of lakes effect whereby discharge from up-gradient lakes contributes to inputs down-gradient, resulting in cumulative isotopic enrichment, because no such spatial patterns in groundwater or surface water were found. A δ_{AO} value of -13‰ was obtained, compared to -16.2‰ based on equilibrium with mean contemporary rainfall.

The percentage of total losses represented by seepage to groundwater was calculated for the case of volumetric and isotopic steady-state within the lake (Gonfiantini, 1986; **Table 3**). Evaporation

index values range from 0.69 to greater than one and good agreement was found between calculations based on $\delta^{18}O$ and δ^2H. The modeled equilibrium steady state value δ_{SS} of +5.6‰ $\delta^{18}O$ is more enriched than approximately half of the sampled lakes, resulting in x-values >1. The most likely reason for exceeding δ_{SS} is a current desiccation trend in those lakes, though whether this reflects seasonal or long-term patterns cannot be deduced without monitoring. Some seasonal lake level variations are apparent and may be attributable to increases in evaporation rates from winter to summer. None of the values approach the estimate for full desiccation (31.3 ‰ $\delta^{18}O$ for h=0.4). Lakes Baddam East, Lexiketu, Baoritalegai South and Baoritalegai North are less enriched than δ_{SS} and have x-values between 0.61 and 0.81, suggesting discharge to groundwater between 19 and 39% of total losses. This reflux to groundwater may help explain the high variability in TDS observed in Badain Jaran shallow groundwater, especially because most wells are located in low lying sites which are near lakes. However, the distinct Na-Cl water type characteristic of the saline lakes (Yang, 2006) is not apparent in groundwater regionally.

6.4 Conceptual Model of Recharge

Based on these tracer data a conceptual model of recharge to the Badain Jaran is proposed (**Fig 9**). During humid climatic phases of the Pleistocene and periods within the early and middle Holocene, surface and groundwater were more abundant in the region (Mischke *et al.*, 2005, Wang *et al.*, 2008, Yang and Williams, 2003, Yuzhen *et al.*, 2003) and the Badain Jaran shallow aquifer was probably replenished by rainfall through a number of mechanisms, including direct and mountain-front recharge. Groundwater discharged to the lowlands to the west and northwest of the desert which also had elevated lake levels during this time, as well as to desert inter-dune lakes. At the end of the mid-Holocene humid phase approximately 6,500 years BP, lake levels and shallow groundwater levels were 15 m higher than at present. Water tables and lake levels fell as inputs diminished because of late Holocene aridification and may continue to do so at a low rate.

Presently, direct infiltration provides approximately 1 mm/yr recharge to the shallow phreatic aquifer, which would be insufficient to support current lake levels and head gradients, although rates of direct recharge are somewhat affected by variability in intensity of the East Asian monsoon (Gates *et al.*, in press). Most recharge originates from the Yabulai Mountains where there is exposed fractured rock and elevated precipitation rates. Shallow groundwater in the Yabulai mountain front is relatively young (in most cases <50 years based on tritium). Groundwater flows towards discharge zones to the west and possibly to the north of the desert. At current hydraulic head gradients, transit time from the recharge zone to the southeastern desert lakes area is approximately 1,000-2,000 yr. However, at this rate remnant palaeo-groundwater from the mid-Holocene humid phase or earlier is likely present further down gradient and along deep flowpaths. Within the southeastern dune area there is cycling between shallow groundwater and lakes, although most of the groundwater that enters the lakes is lost to evaporation. Deeper confined groundwater is not connected to the shallow system and consistently has residence times in the thousands of years and as early as the Pleistocene.

Figure 9 Conceptual diagram of recharge to the southeastern Badain Jaran Desert

7 Conclusions

Recharge mechanisms and timing for the southeastern Badain Jaran Desert have been considered on the basis of multiple isotopic and chemical tracers. Several key aspects of the system are elucidated by the available data:

1. Enriched stable isotope signatures in the unsaturated zone confirm previous results from Cl mass balance that direct infiltration of precipitation is not a volumetrically-important source of recharge to the shallow aquifer in the southeastern desert margin. The unsaturated zone

evaporation line has slope 2.4 and has a LMWL origin similar to that of modern precipitation, distinct from shallow groundwater with a slope of 4.5 and a more depleted LMWL intercept.

2. An ESE-WNW trending flowpath from the Yabulai mountain front is discernable on the basis of water table elevations, and supported by stable isotope and chemical compositions, suggesting the Yabulai Mountains as the dominant recharge source location to the southeastern portion of the desert. Additional evidence includes modern radiocarbon activities, high tritium, and presence of perennial surface water near the mountain front.

3. Shallow groundwater is chemically and isotopically distinct from deeper confined sources, suggesting minimal connection between them.

4. Radiocarbon dating suggests a residence time of 1,600 years for the shallow unconfined desert groundwater near Baddam Lake. Deep confined groundwaters generally have residence times in the thousands to tens of thousands of years.

Although physical characterization of the aquifer system remains coarse due to a lack of data in the region, these results imply that inputs to the Badain Jaran Desert's shallow aquifer are currently low and would therefore be sensitive to increased abstraction, as well as continuing decline due to natural processes of aridification. Judging by lake levels that appear to be in slow long-term decline, current water table elevations may represent a diminishing piezometric system which can be interpreted as an ongoing response to late-Holocene aridification. Declining groundwater and lake levels endanger a valuable desert ecosystem and a growing potential for income from tourism. Further refinement of this conceptual model will be difficult without drilling and detailed characterization of the physical system.

Acknowledgements

Figure Captions

Figure 1 Map of groundwater sample locations

Figure 2 Lake level contours (50 m) in the southeastern Badain Jaran

Figure 3a Piper diagram comparing Badain Jaran, Yabulai mountain front and rainfall samples

Figure 3b Piper diagram comparing deep and shallow groundwater samples

Figure 4 $\delta^{18}O$ - δ^2H diagram

Figure 5a Groundwater Na/Cl cross-plot

Figure 5b Groundwater SO_4/Cl cross-plot

Figure 6 Monthly weighted mean isotope compositions for Zhangye GNIP station (icon size scaled to monthly amounts)

Figure 7 $\delta^{18}O$ versus pmC (including data from Edmunds et al 2006). Values for samples which have been subject to evaporation have been adjusted to reflect original meteoric water.

Figure 8 Groundwater $\delta^{13}C_{DIC}$/pmC cross-plot

Figure 9 Conceptual diagram of recharge to the southeastern Badain Jaran Desert

Sample	Category	Z (m)	pH	T (°C)	TDS (g/L)	O_2	Ca	Na	Mg	K	Cl	NO_3 ppm	SO_4	HCO_3	Mn	Fe	δ^2H ‰ VSMOW	$\delta^{18}O$
W1	Deep	140	7.7	14.5	1.88	4.2	237	108	155	15	700	8	540	122	0.008	0.149	-69.1	-9.4
W4	Deep	150	8.0	15.5	2.97	1.7	159	759	73	16	875	1	1000	80	0.366	7.898	-68.1	-8.5
W5	Deep	80	8.0	16.4	0.83	5.8	67	174	33	6	205	13	193	133	0.005	0.135	-70.0	-8.8
W6	Deep	-	8.4	19.3	0.55	2.6	23	152	11	4	90	7	153	107	0.004	0.129	-91.5	-12.0
W17	Deep	-	8.3	11.3	1.96	11.7	27	668	21	5	590	14	490	143	0.002	0.084	-81.1	-11.3
W19	Deep	230	7.6	13.8	2.17	6.8	171	539	26	6	560	19	680	171	0.002	0.078	-70.9	-9.7
W20	Deep	225	7.9	-	1.78	-	47	476	49	4	385	22	610	188	0.004	0.072	-82.5	-11.1
W22	Deep	-	7.8	16.4	1.48	5.6	66	409	21	4	340	19	440	174	0.006	0.070	-72.6	-9.7
W23	Deep	-	8.1	14.2	0.78	9.3	50	192	12	2	135	21	265	104	0.001	0.076	-86.3	-11.6
W24	Deep	-	7.9	14.7	2.24	5.1	101	568	47	4	580	8	790	140	0.003	0.080	-85.7	-10.4
W25	Deep	80	8.2	13.2	1.05	5.9	62	289	3	4	190	33	390	73	0.001	0.092	-84.2	-10.8
W26	Deep	80	7.9	10.9	2.87	3.3	76	675	120	22	663	6	1113	190	0.005	0.098	-73.3	-10.9
W27	Deep	150	7.9	14.3	3.08	-	510	220	193	8	395	24	1625	110	0.010	0.162	-	-
W28	Deep	150	7.9	14.3	0.44	-	52	36	26	3	36	8	98	182	0.001	0.074	-59.6	-9.5
W29	Deep	140	7.8	11.6	0.58	-	74	44	30	3	70	36	108	220	0.001	0.069	-56.4	-9.4
W37	Deep	-	7.8	12.1	1.21	8.7	39	274	39	11	346	45	297	162	0.003	0.037	-63.1	-6.6
W43	Deep	144	8.6	20.8	0.62	5.2	10	173	11	13	118	18	119	154	0.001	0.018	-58.4	-4.5
W2	Southern Margin Shallow	3	7.5	19.5	1.00	2.3	91	197	36	8	195	2	245	220	0.567	0.594	-52.4	-7.1
W3	Southern Margin Shallow	3	7.8	21.1	1.16	6.4	71	279	11	1	243	23	310	213	0.006	0.144	-71.9	-9.3
W11	Southern Margin Shallow	-	7.8	17.8	2.65	8.8	147	730	17	3	730	6	920	95	0.007	0.147	-75.8	-9.0
W12	Southern Margin Shallow	1.5	8.1	15.4	1.32	9.0	72	324	31	4	320	40	305	220	0.007	0.074	-64.2	-9.0
W13	Southern Margin Shallow	2	8.1	16.8	3.57	9.0	111	987	46	9	1025	93	1100	195	0.003	0.084	-59.9	-6.8
W14	Southern Margin Shallow	-	8.1	17.2	0.58	4.6	35	116	15	10	82	46	99	177	<0.001	0.061	-39.0	-6.6
W15	Southern Margin Shallow	2	8.0	18	2.12	6.0	50	620	26	7	590	26	500	298	0.002	0.068	-63.4	-8.9
W16	Southern Margin Shallow	1	8.0	15.7	2.13	-	66	553	64	7	495	54	730	159	0.003	0.088	-56.3	-8.0
W18	Southern Margin Shallow	-	8.3	16.6	0.98	8.8	30	178	56	8	143	48	225	293	0.002	0.079	-55.9	-8.8
W21	Southern Margin Shallow	4	7.5	18.8	2.29	4.8	140	549	60	4	600	29	710	195	0.012	0.080	-58.6	-8.4
S1	Southern Margin Spring	n/a	8.1	15.4	1.33	9.0	30	385	10	1	306	35	285	271	0.005	0.060	-72.9	-9.4
S2	Southern Margin Spring	n/a	8.2	14.2	2.12	11.0	57	543	63	8	435	54	700	256	0.002	0.083	-53.1	-8.2
W7	Mountain Front Shallow	7	8.0	10.1	1.12	8.6	102	177	51	6	270	88	265	159	0.006	0.010	-59.2	-7.9
W8	Mountain Front Shallow	1	7.7	13.9	3.11	5.7	139	728	108	12	776	85	1098	162	0.010	0.010	-52.8	-5.6
W9	Mountain Front Shallow	2	7.7	19.2	0.58	5.5	38	97	13	17	45	54	130	182	0.002	0.017	-46.9	-6.9
W10	Mountain Front	3	7.3	16.8	1.57	5.5	88	355	45	8	343	30	509	190	0.004	0.043	-57.5	-8.1

W30	Shallow Mountain Front Shallow	1	8.2	22.4	4.67	6.4	219	1309	175	22	1366	<1	1340	238	0.012	0.107	-30.3	-1.8
W31	Mountain Front Shallow	2	8.0	20.5	2.39	6.6	126	668	48	1	750	31	620	142	0.005	0.048	-44.5	-4.9
W32	Mountain Front Shallow	-	6.0	15.8	1.39	0.6	91	274	43	5	305	12	421	233	0.015	0.048	-56.2	-7.9
W33	Mountain Front Shallow	2	7.7	17.9	2.39	4.9	133	489	83	28	585	36	820	203	0.007	0.074	-58.8	-7.6
W34	Mountain Front Shallow	1	8.2	19.6	1.68	3.3	29	417	28	20	266	113	414	389	0.002	0.030	-44.8	-4.6
W35	Xugue Shallow	2	7.8	18.4	0.73	3.7	46	152	13	1	98	53	155	213	0.001	0.019	-59.0	-7.2
W36	Xugue Shallow	-	7.5	16.6	0.80	3.2	52	144	26	8	128	68	141	229	0.003	0.032	-50.7	-4.7
W38	Xugue Shallow	8	7.6	16.5	0.72	5.8	35	123	26	25	109	60	108	230	0.002	0.032	-51.2	-5.0
W39	Xugue Shallow	1	7.7	19.6	2.17	1.2	43	579	46	17	486	6	471	522	0.004	0.044	-50.0	-4.4
W41	Gurinai Shallow	1	8.0	16.5	0.58	5.2	13	147	9	8	86	38	115	157	<0.001	0.014	-36.7	-1.3
W42	Gurinai Shallow	2	8.0	14.4	0.99	5.7	22	259	15	17	157	14	194	304	0.002	0.018	-54.6	-4.0
W44	Gurinai Shallow	1	7.4	15.5	1.09	2.7	36	254	25	9	184	<1	316	260	0.010	0.026	-46.1	-2.7
WBD1	Badain Jaran Shallow	<1	-	-	0.64	-	61	130	16	10	108	47	100	171	0.009	0.085	-40.1	-2.6
WBD2	Badain Jaran Shallow	<1	-	-	-	-	-	-	-	-	-	-	-	-	0.004	0.095	-39.5	-2.7
WBD3	Badain Jaran Shallow	<1	-	-	1.14	-	30	264	38	38	165	80	203	305	0.003	0.090	-42.0	-2.4
WBD4	Badain Jaran Shallow	3	-	-	0.75	-	34	166	24	10	155	60	173	122	0.003	0.026	-54.2	-3.7
WBD5	Badain Jaran Shallow	83	8.4	15.1	0.81	6	41	170	21	10	151	81	180	156	0.160	1.278	-47.4	-3.9
WBD6	Badain Jaran Shallow	21	-	-	1.81	-	80	384	88	26	525	1	495	207	0.012	0.181	-28.1	0.1
WBD7	Badain Jaran Shallow	1	-	-	0.96	-	83	173	29	11	193	49	173	250	0.012	0.170	-43.5	-3.9
SBD8	Badain Jaran Shallow	n/a	-	-	1.31	-	34	313	53	17	365	1	305	226	0.003	0.124	-13.4	4.6
WBD9	Badain Jaran Shallow	<1	-	-	0.63	-	29	119	24	11	105	98	90	152	0.001	0.088	-39.0	-2.0
SBD10	Badain Jaran Shallow	n/a	-	-	0.43	-	19	82	15	9	53	30	65	159	0.002	0.090	-53.2	-5.2
SBD11	Badain Jaran Shallow	n/a	-	-	0.39	-	13	80	8	6	40	28	43	171	0.083	0.349	-54.3	-4.5
WBD12	Badain Jaran Shallow	3	-	-	0.79	-	52	155	35	15	143	1	195	195	0.002	0.055	-55.9	-5.4
WBD13	Badain Jaran Shallow	1	-	-	0.46	-	24	78	21	17	68	51	65	134	0.031	0.531	-58.3	-4.7
W40	Badain Jaran Shallow	1	7.4	17.9	6.08	2.2	70	1971	36	4	1451	74	1854	623	0.055	0.047	-50.5	-3.9
Rain1	Precipitation	n/a	-	-	-	-	6	4	1	1	21	8	17	21	0.002	0.048	-15.9	-2.4
Rain2	Precipitation	n/a	-	-	-	-	-	-	-	-	-	-	-	-	0.006	0.071	-29.5	-4.8
Rain3	Precipitation	n/a	-	-	-	-	2	8	0	1	7.0	1.0	3.0	18.29	0.008	0.149	-32.0	-4.8
Rain4	Precipitation	n/a	-	-	-	-	12	11	6	8	4	1	4	27	0.567	0.594	8.2	0.6

Table 1 Field data, ions concentrations and stable isotopes in groundwater and rainfall

Sample	Category	^{3}H TU	^{14}C (pmC)	δ^{13}C (‰ PDB)	Uncorrected Age (Years)	Isotope Balance (Years)	q	SI (CaCO$_3$)
W1	Deep	-	27.5	-6.4	10669	7472	0.68	+0.37
W5	Deep	-	33.9	-9.3	8955	8556	0.95	+0.33
W17	Deep	-	17.7	-6.3	14319	11007	0.67	+0.06
W19	Deep	-	14.3	-7.3	16101	13878	0.76	+0.25
W20	Deep	-	15.0	-5.6	15688	11518	0.60	+0.14
W23	Deep	-	2.7	-6.7	29889	27030	0.71	+0.16
W25	Deep	-	3.1	-7.6	28824	26902	0.79	+0.13
W26	Deep	-	4.1	-6.9	26507	23865	0.73	+0.13
W27	Deep	-	49.2	-13.2	5857	8157	1.32	+0.71
W28	Deep	-	37.8	-6.7	8051	5191	0.71	+0.30
W29	Deep	-	72.5	-6.3	2655	-658	0.67	+0.37
W37	Deep	0.0	47.7	-7.3	6128	4160	0.79	-0.13
W43	Deep	0.0	11.5	-4.5	17901	12972	0.55	+0.25
W8	Mountain Front Shallow	12.1	77.5	-7.7	2105	485	0.82	+0.16
W9	Mountain Front Shallow	21.9	90.9	-8.9	791	136	0.92	+0.01
W10	Mountain Front Shallow	15.0	82.0	-8.2	1644	439	0.86	-0.20
W33	Mountain Front Shallow	15.3	90.1	-9.5	859	646	0.97	+0.35
W34	Mountain Front Shallow	43.2	96.9	-9.8	258	258	1.00	+0.55
W44	Gurinai Shallow	1.4	68.1	-6.5	3176	464	0.73	-0.30
W40	Badain Jaran Shallow	39.4	101.8	-10.1	-143	64	1.03	+0.08
WBD5	Badain Jaran Shallow	0.0	59.8	-6.6	4248	1633	0.73	+0.55

Table 2 Tritium and carbon isotope results and modeled radiocarbon ages

Lake	δ^2H (‰ VSMOW)	$\delta^{18}O$	X (δ^2H)	X ($\delta^{18}O$)
Sayin Wusu East	11.2	8.1	1.21	1.18
Sayin Wusu West	7.6	8.1	1.12	1.18
Baddam East	-4.5	5.9	0.88	0.96
Baddam West	22.9	11.8	1.50	1.66
Nouertu	8.8	7.0	1.15	1.07
Lexiketu	-10.2	2.7	0.78	0.69
Baoritalegai South	-10.7	4.3	0.77	0.82
Baoritalegai North	0.8	6.0	0.97	0.97
Yindertu	0.2	7.6	0.97	1.13
Huhejaran	2.7	7.1	1.02	1.07
Suhaitu	-12.0	5.1	0.74	0.89

Table 3 Stable isotope results for lakes and modeled evaporation indices
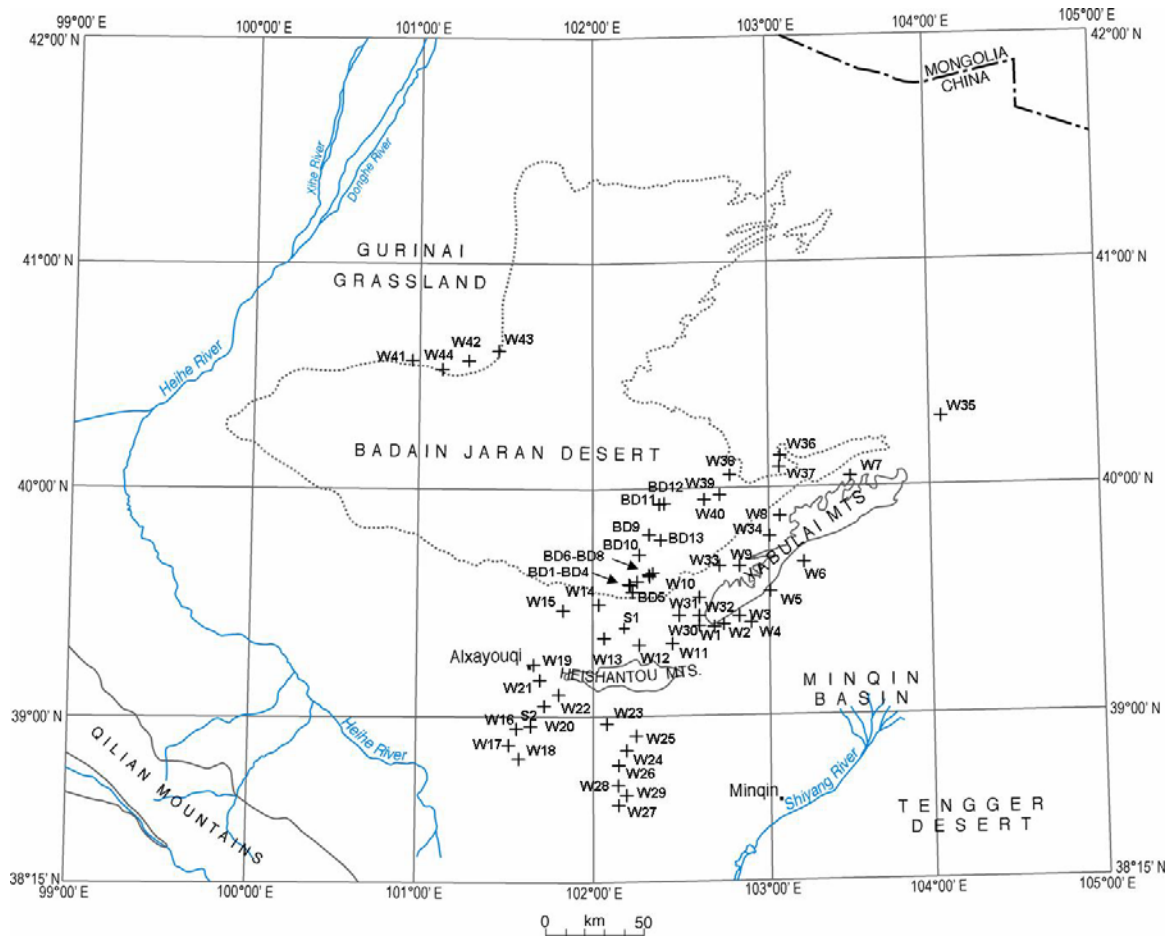
Fig 1

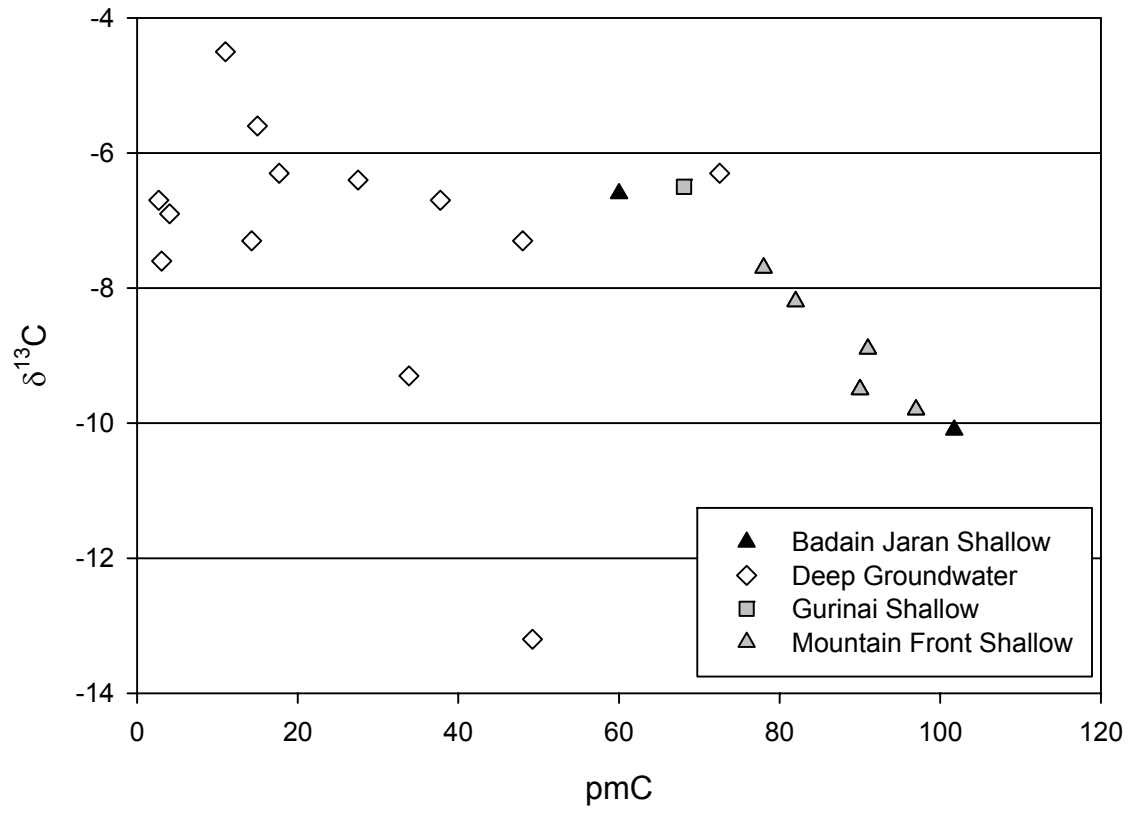Fig 2
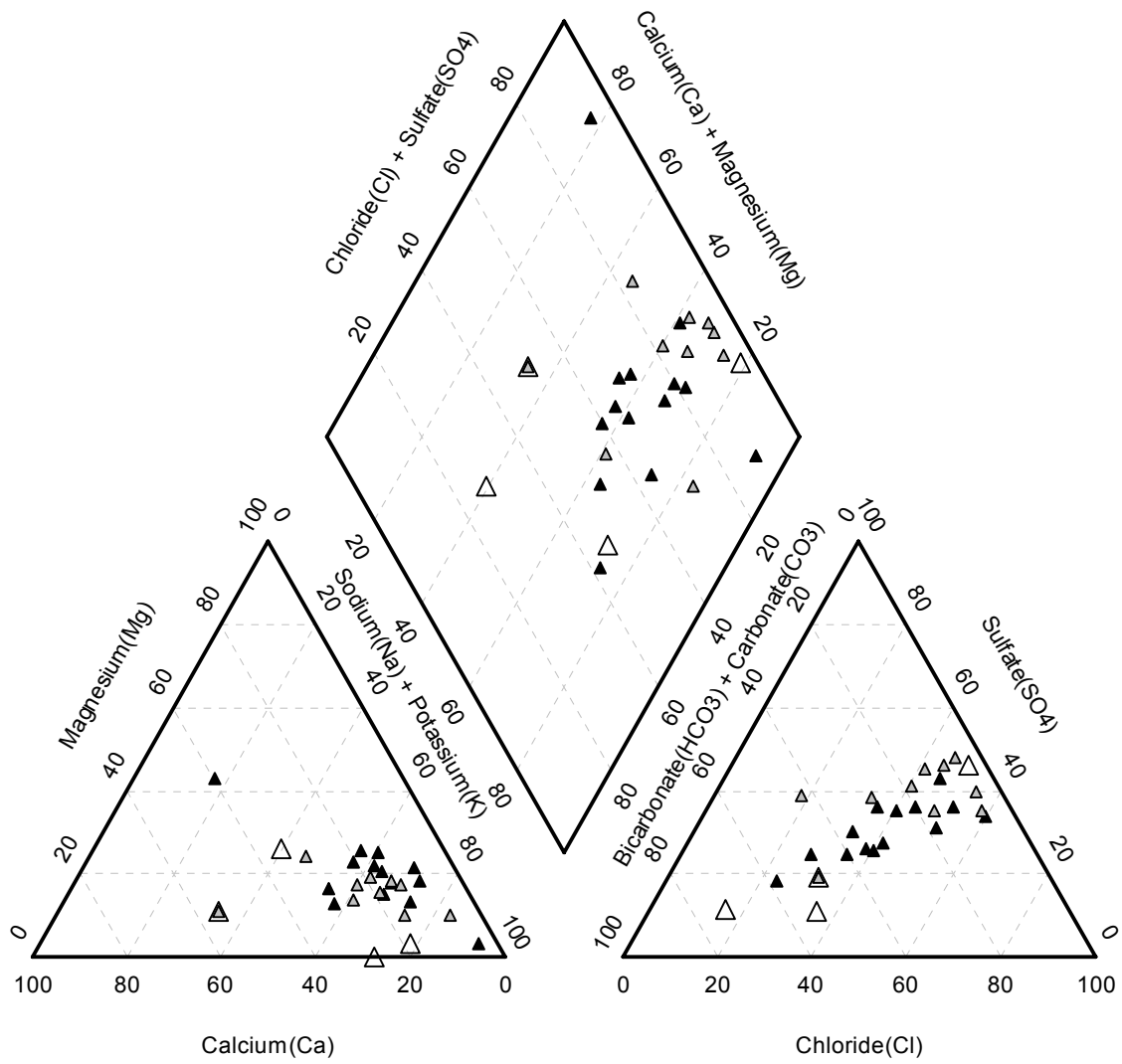
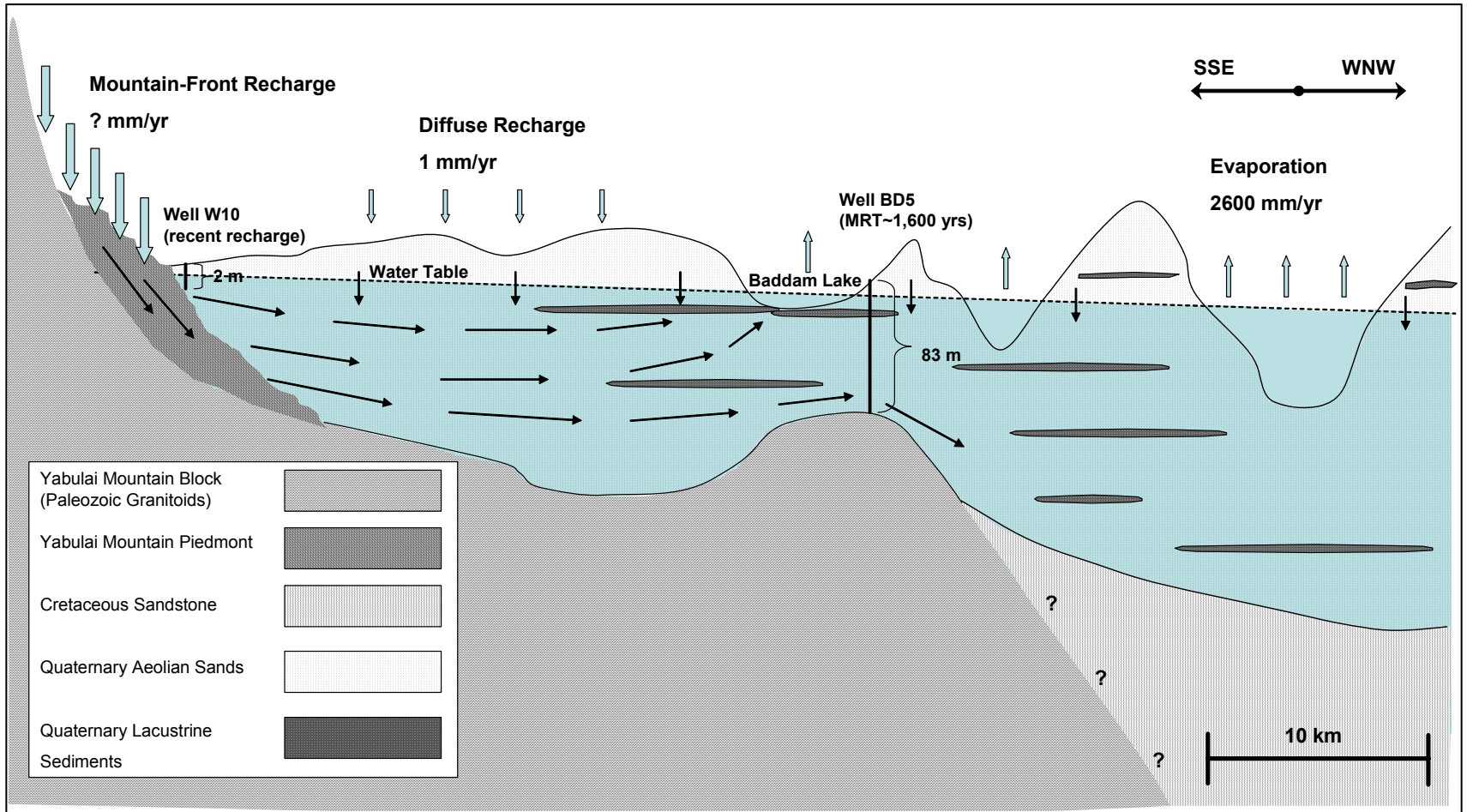Fig 3a
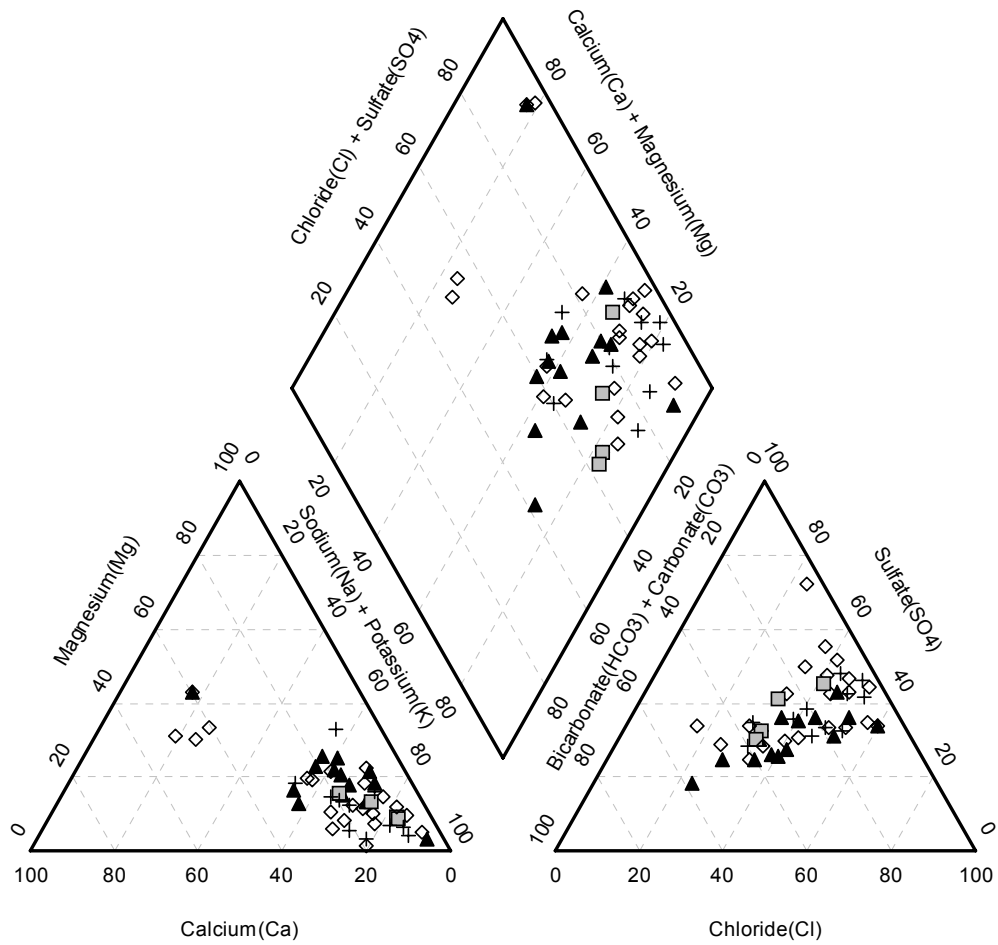
Fig 3b
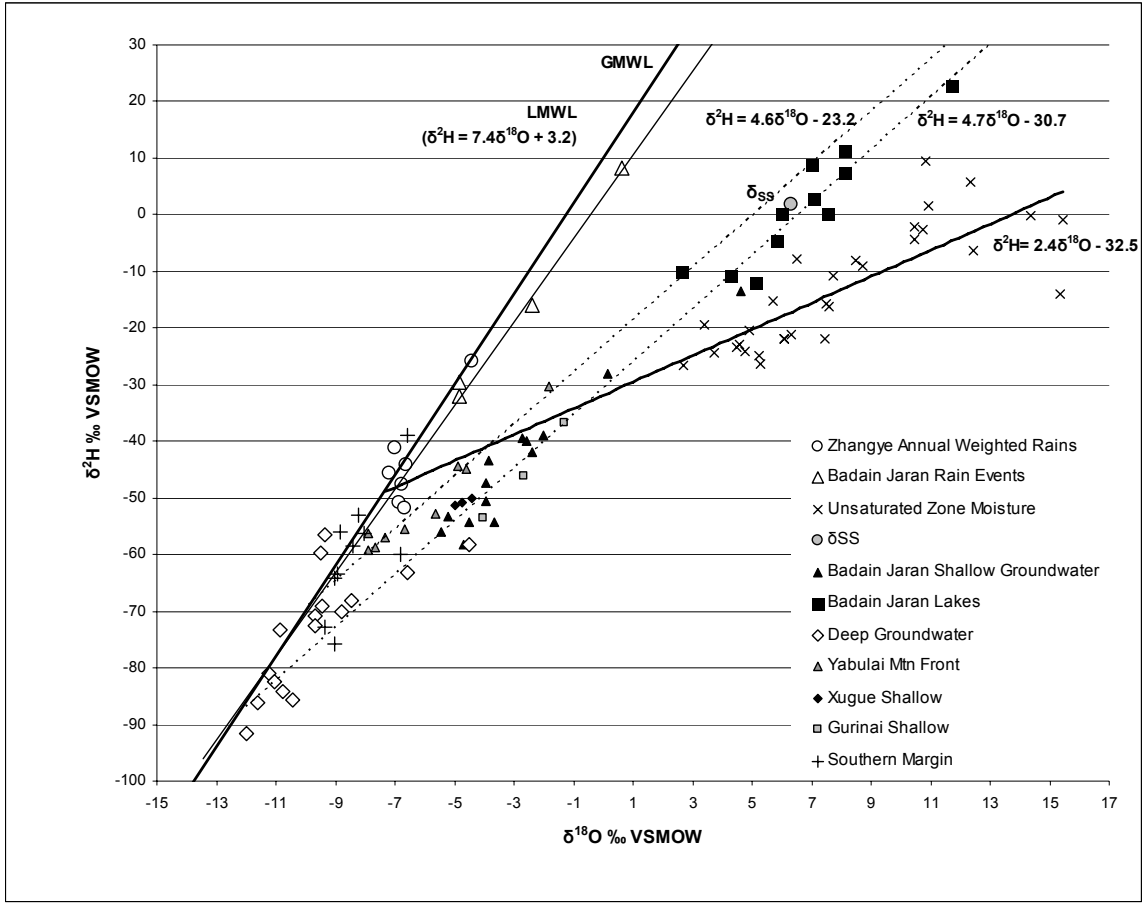
Fig 4
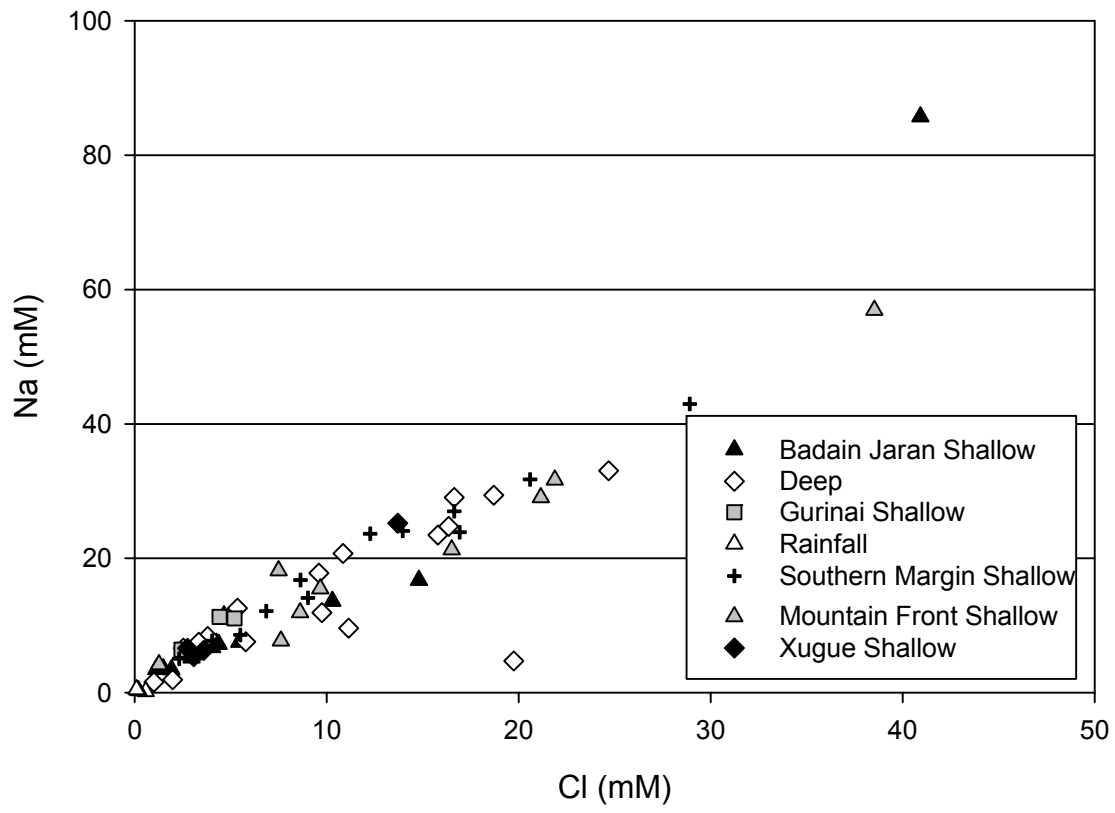
Fig 5a
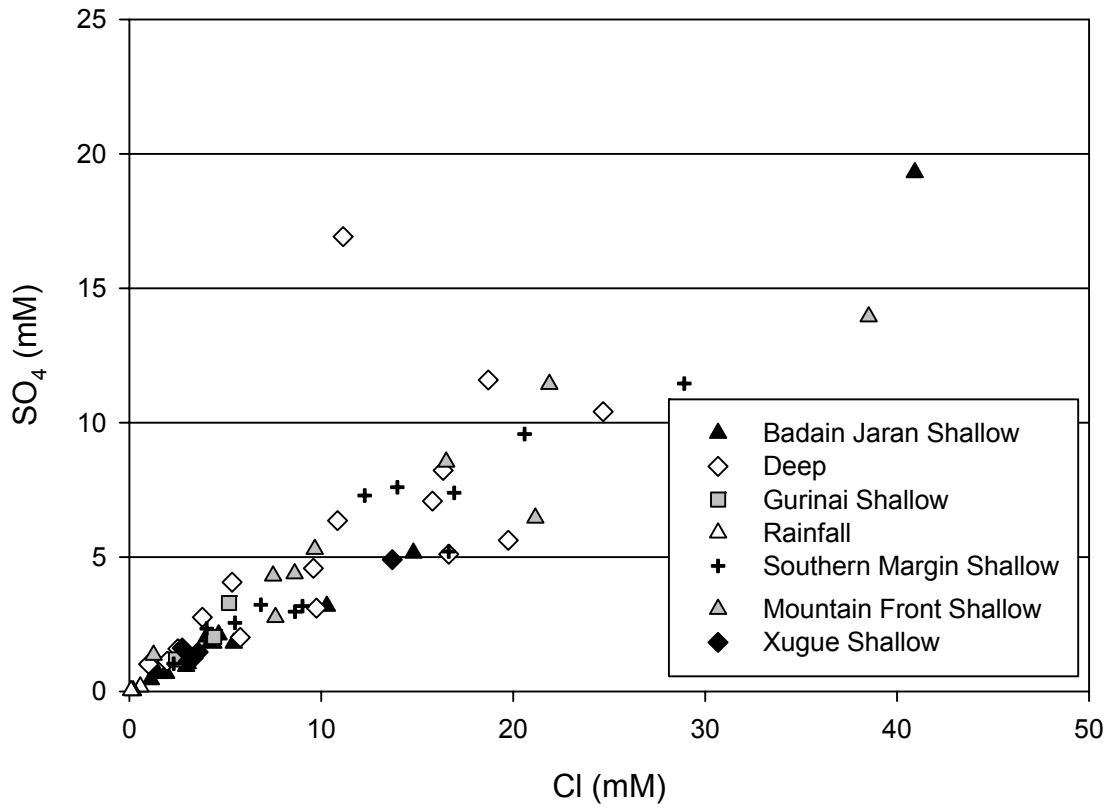
Fig 5b
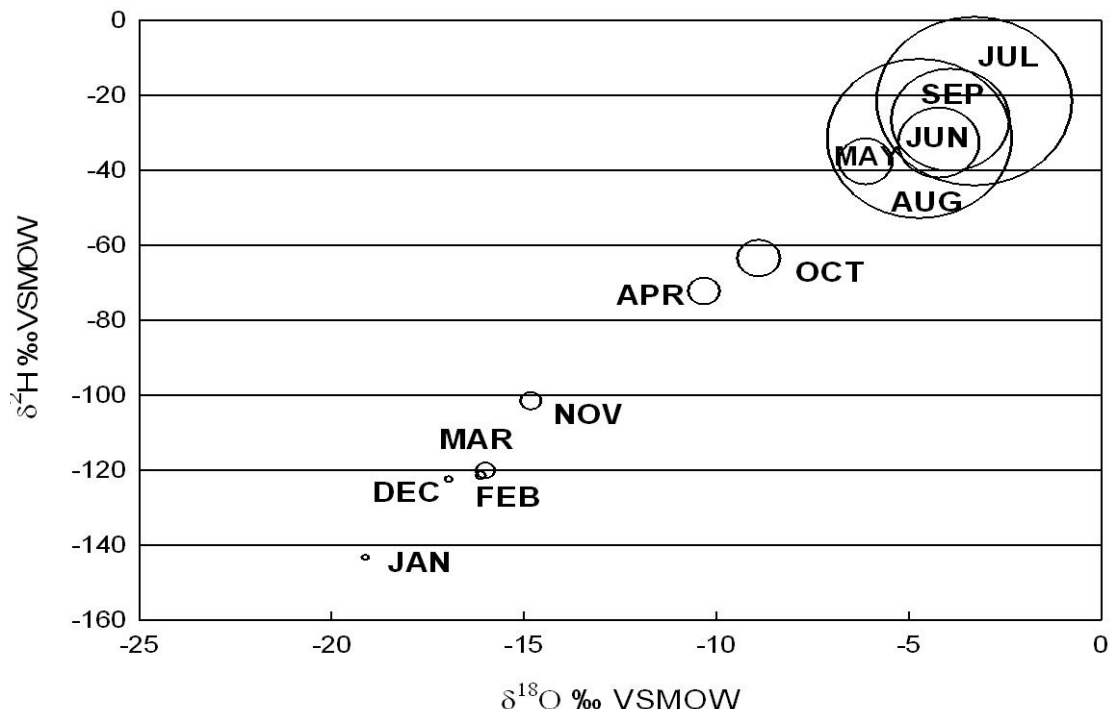
Fig 6
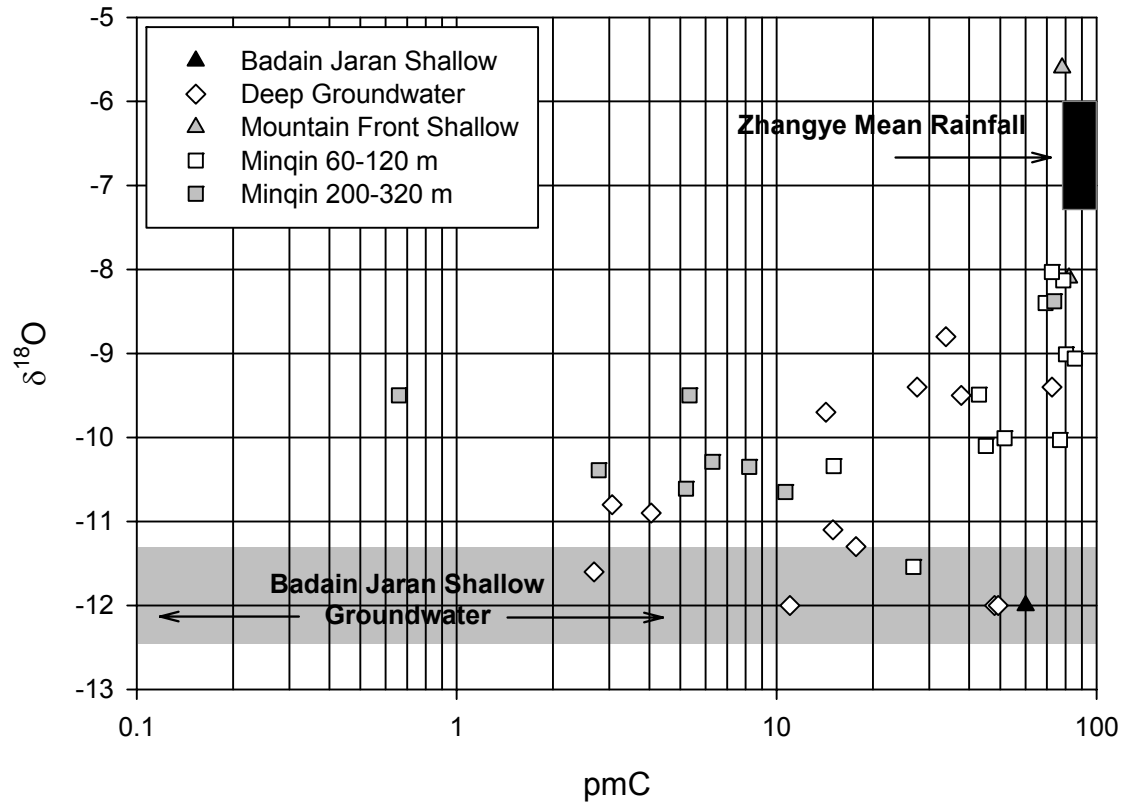
Fig 7

Fig 8

Fig 9

References

An, Z., Porter, S.C., Kutzbach, J.E., Wu, X., Wang, S., Liu, X., Li, X., Zhou, W., 2000. Asynchronous Holocene optimum of the East Asian monsoon. Quaternary Science Reviews 19, 743-762.

Aravena, R., Schiff, S.L., Trumbore, S.E., Dillon, P.J., Elgood, R., 1992. Evaluating dissolved inorganic carbon cycling in a forested lake watershed using carbon isotopes. Radiocarbon 34, 1-10.

Barnes, C.J., Allison, G.B., 1988. Tracing of water movement in the unsaturated zone using stable isotopes of hydrogen and oxygen. Journal of Hydrology 100, 143-176.

Chen, J.S., Li, L., Wang, J.Y., Barry, D.A., Sheng, X.F., Gu, W.-Z., Zhao, X., Chen, L., 2004. Groundwater maintains dune landscape. Nature 432, 459-460.

Chen, Z., Nie, Z., Zhang, G., Wan, L., Shen, J., 2006. Environmental isotopic study on the recharge and residence time of groundwater in the Heihe River Basin, northwestern China. 14, 1635–1651.

Clark, I., Fritz, P., 1997. Environmental Isotopes in Hydrogeology CRC Press/Lewis Publishers, Boca Raton.

Domros, M., Peng, G., 1988. The Climate of China. Springer, Berlin.

Dong, Z., Wang, T., Wang, X., 2004. Geomorphology of the megadunes in the Badain Jaran Desert. Geomorphology 60, 203.

Edmunds, W.M., Ma, J., Aeschbach-Hertig, W., Kipfer, R., Darbyshire, F., 2006. Groundwater recharge history and hydrogeochemical evolution in the Minqin Basin, North West China. Applied Geochemistry 21, 2148-2170.

Feng, Q., Liu, W., Su, Y.H., Zhang, Y.W., Si, J.H., 2004. Distribution and evolution of water chemistry in Heihe River basin. Environmental Geology 45, 947-956.

Gao, Q., Tao, Z., Li, B., Jin, H., Zou, X., Zhang, Y., Dong, G., 2006. Palaeomonsoon variability in the southern fringe of the Badain Jaran Desert, China, since 130 ka BP. Earth Surface Processes and Landforms 31, 265-283.

Gat, J.R., 1996. Oxygen and hydrogen isotopes in the hydrologic cycle. Annual Review of Earth and Planetary Sciences 24, 225-262.

Gat, J.R., Levy, Y., 1978. Isotope hydrology and inland sabkhas in the Bardawil area, Sinai. Limnology and Oceanography 23, 841-850.

Gates, J.B., Böhlke, J.K., Edmunds, W.M., 2008. Ecohydrological Factors Affecting Nitrate Concentrations in a Phreatic Desert Aquifer in Northwestern China. Environmental Science and Technology 42, 3531-3537.

Gates, J.B., Edmunds, W.M., Ma, J., Scanlon, B.R., in press. Estimating groundwater recharge in a cold desert environment in northern China using chloride. Hydrogeology Journal.

Geyh, M.A., Gu, W.Z., 1992. Preliminary isotope hydrological study in the arid Gurinai grassland area, Inner Mongolia. In: Isotope Techniques in Water Resources Development 1991. IAEA, Vienna.

Gibson, J.J., Edwards, T.W.D., Prowse, T.D., 1999. Pan-derived isotopic composition of atmospheric water vapour and its variability in northern Canada. Journal of Hydrology 217, 55-74.

Gonfiantini, R., 1986. Environmental isotopes in lakes studies. In: Fritz, P., Fontes, J.C. (Eds.), Handbook of Environmental Isotope Geochemistry, Vol. 2, The Terrestrial Environment. Elsevier, Amsterdam, pp. 113-168.

Hofmann, J., 1999. Geoökologische Untersuchungen der Gewässer im Südosten der Badain Jaran Wüste. Berliner Geographische Abhandlungen 64, 247.

Horita, J., Wesolowski, D.J., 1994. Liquid-vapor fractionation of oxygen and hydrogen isotopes of water from the freezing to the critical temperature. Geochimica et Cosmochimica Acta 58, 3425-3437.

IAEA/WMO, 2007. Global Network of Isotopes in Precipitation. http://isohis.iaea.org.

Jäkel, D., 2002. The importance of dunes for groundwater recharge and storage in China. Zeitschrift Fur Geomorphologie Supplementband 126, 131-146.

Krabbenhoft, D.P., Bowser, C., Anderson, M.J.P., Valley, J.W., 1990. Estimating Groundwater Exchange With Lakes 1. The Stable Isotope Mass Balance Method. Water Resources Research 26, 2445-2453.

Kürschner, H., 2004. Phytosociological studies in the Alashan Gobi - A contribution to the flora and vegetation of Inner Mongolia (NW China). Phytocoenologia 34, 169-224.

Ma, J., Edmunds, W.M., 2006. Groundwater and lake evolution in the Badain Jaran desert ecosystem, Inner Mongolia. Hydrogeology Journal 14, 1231-1243.

Ma, J., Edmunds, W.M., Chen, F., 2003. Groundwater geochemistry evolution and unsaturated zone archives of climatic change in arid NW China. In: XVI INQUA congress; Shaping the Earth; a Quaternary perspective. pp. 177-178.

Ma, J.Z., Ding, Z., Gates, J.B., Su, Y., in press. Chloride and the environmental isotopes as the indicators of the groundwater recharge in the Gobi Desert, northwest China. Environmental Geology.

Masch, F.D., Denny, K.J., 1966. Grain size distribution and its effect on the permeability of unconsolidated sands. Water Resources Research 4, 665-677.

Mischke, S., Demske, D., Wünnemann, B., Schudack, M., 2005. Groundwater discharge to a Gobi desert lake during Mid and Late Holcene dry periods. Palaeogeography, Palaeoclimatology, Palaeoecology 225, 157-172.

Mook, W.G., Bommerson, J.C., Staverman, W.H., 1974. Carbon isotope fractionation between dissolved bicarbonate and gaseous carbon dioxide. Earth and Planetary Science Letters 22, 169-176.

Pang, Z., Qin, D., Yang, Y., 2007. Isotopes in deep groundwater in Northwest China: Hydrological and paleoclimate implications. In: International Symposium on Advances in Isotopes Hydrology and its Role in Sustainable Water Resources Management. IAEA Vienna.

Parkhurst, D.L., 1995. Users guide to PHREEQC: A computer program for speciation, reaction-path, advective-transport, and inverse geochemical calculations. In: USGS Water-Resources Investigation Report 95-4227.

Pearson, F.J., 1965. Use of C-13/C-12 ratios to correct radiocarbon ages of material initially diluted by limestone. In: Proceedings of the 6th International Conference on Radiocarbon and Tritium Dating. Pullman, WA, pp. 357.

Pyankov, I.P., Gunin, P.D., Tsoog, S., Black, C.C., 2000. C4 plants in the vegetation of Mongolia: their natural occurrence and geographical distribution in relation to climate. Oecologia 123, 15-31.

Revesz, K., Woods, P.H., 1990. A method to extract soil water for stable isotope analysis. Journal of Hydrology 115, 397-406.

Rozanski, K., Araguas-Araguas, L., Gonfiantini, R., 1993. Isotopic patterns in modern global precipitation. In: Swart, P.K., Lohwan, K.L., McKenzie, J.A., Savin, S. (Eds.), Climate Change in Continental Isotopic Record. American Geophysical Union, Washington DC, pp. 1-37.

Thompson, L., Tandong, Y., Davis, M.E., Mosley-Thompson, E., Mashiotta, T.A., Lin, P.N., Mikhalenko, V.N., Zagorodnov, V.S., 2006. Holocene climate variability archived in the Puruogangri ice cap on the central Tibetan Plateau. Annals of Glaciology 43, 61-69.

Turner, J.V., 1982. Kinetic fractionation of carbon-13 during calcium carbonate precipitation. Geochimica et Cosmochimica Acta 46, 1183-1191.

Vincent, S.J., Allen, M.B., 1999. Evolution of the Minle and Chaoshui Basins, China: Implications for Mesozoic strike-slip basin formation in Central Asia. GSA Bulletin 111, 725-742.

Vogel, 1993. Variability of carbon isotope fractionation during photosynthesis. In: Ehleringer, J.R., Hall, A.E., Farquhar, G.D. (Eds.), Stable Isotopes and Plant Carbon - Water Relations. Academic Press, San Diego, pp. 29-38.

Vogel, J.C., 1970. Carbon-14 dating of groundwater. In: Isotope Hydrology 1970. IAEA Vienna, pp. 225-239.

Wang, R., 2007. C4 plants in the deserts of China: occurrence of C4 photosynthesis and its morphological functional types. Photosynthetica 45, 167-171.

Wang, X., Chen, F., Hasi, E., Li, J., 2008. Desertification in China: An assessment. Earth-Science Reviews 88, 188-206.

Wen, X., Wu, Y., Su, J., Zhang, Y., Liu, F., 2005. Hydrochemical characteristics and salinity of groundwater in the Ejina Basin, Northwestern China. Environmental Geology 48, 665-675.

Wigley, T.M.L., Plummer, L.N., Pearson, F.J., 1978. Mass transfer and carbon isotope evolution in natural water systems. Geochimica et Cosmochimica Acta 42, 1117-1139.

Yan, M., Wang, S., Li, B., Dong, G., 2001. Formation and growth of high megadunes in Badain Jaran Desert. Acta Geographica Sinica 56, 83-91.

Yang, X., 2006. Chemistry and late Quaternary evolution of ground and surface waters in the area of Yabulai Mountains, western Inner Mongolia, China Catena 66, 135-144.

Yang, X., 2000. Landscape evolution and precipitation changes in the Badain Jaran Desert during the last 30,000 years. Chinese Sciences Bulletin 45, 1042-1047.

Yang, X., Rost, K.T., Lehmkuhl, F., Zhenda, Z., Dodson, J., 2004. The evolution of dry lands in northern China and in the Republic of Mongolia since the Last Glacial Maximum. Quaternary International 118-199, 69-85.

Yang, X., Williams, M.A.J., 2003. The ion chemistry of lakes and late Holocene desiccation in the Badain Jaran Desert, Inner Mongolia, China. Catena 51, 45-60.

Yuzhen, M., Hucai, Z., Pachur, H.J., Wunemann, B., Jijun, L., Zhaodong, F., 2003. Late glacial and holocene vegetation history and paleoclimate of the Tengger Desert, northwestern China. Chinese Science Bulletin 48.

Zhang, Y., Wu, Y., Su, J., Wen, X., Liu, F., 2005. Groundwater replenishment analysis by using natural isotopes in Ejina Basin, Northwestern China. Environmental Geology 48, 6-14.

Zhao, S., 1986. Physical Geography of China. Beijing Science Press, Beijing.

Zhou, W., Head, M.J., Deng, L., 2001. Climate changes in northern China since the late Pleistocene and its response to global change. Quaternary International 83-85, 285-292.

Zongyu, C., Jixiang, Q., Jianming, X., Jiaming, X., Hao, Y., Yunju, N., 2003. Paleoclimatic interpretation of the past 30 ka from isotopic studies of the deep confined aquifer of the North China plain. Applied Geochemistry 18, 1009.